INSTITUTE OF PHYSICS PUBLISHING PLASMA PHYSICS AND CONTROLLED FUSION

Plasma Phys. Control. Fusion **43** (2001) 743–759 www.iop.org/Journals/pp PII: S0741-3335(01)22467-1

Thermodynamics of hot dense H-plasmas: path integral Monte Carlo simulations and analytical approximations

V S Filinov[1], M Bonitz[2], W Ebeling[3] and V E Fortov[1]

[1] Russian Academy of Sciences, High Energy Density Research Center, Izhorskaya street 13–19, Moscow 127412, Russia
[2] Fachbereich Physik, Universität Rostock, Universitätsplatz 3, D-18051 Rostock, Germany
[3] Institut für Physik, Humboldt-Universität Berlin, Invalidenstrasse 110, D-10115 Berlin, Germany

Received 5 March 2001

Abstract

This work is devoted to the thermodynamics of high-temperature dense hydrogen plasmas in the pressure region between 10^{-1} and 10^{2} Mbar. In particular, we present for this region results of extensive calculations based on a recently developed path integral Monte Carlo scheme (direct PIMC). This method allows for a correct treatment of the thermodynamic properties of hot dense Coulomb systems. Calculations were performed in a broad region of the non-ideality parameter $\Gamma \lesssim 3$ and degeneracy parameter $n_e\Lambda^3 \lesssim 10$. We give a comparison with a few available results from other path integral calculations (restricted PIMC) and with analytical calculations based on Padé approximations for strongly ionized plasmas. Good agreement between the results obtained from the three independent methods is found.

1. Introduction

The thermodynamics of strongly correlated Fermi systems at high pressures are of growing importance in many fields, including shock and laser plasmas, astrophysics, solids and nuclear matter, see [1–4] for an overview. In particular, the thermodynamical properties of hot dense plasmas under high pressure are of importance for the description of plasmas relevant for laser fusion [5]. Further among the phenomena of current interest are Fermi liquids, metallic hydrogen [6], plasma phase transition, see for example [7] and references therein, bound states etc, which occur in situations where both Coulomb *and* quantum effects are relevant. There has been significant progress in recent years to study these systems analytically and numerically, see for example [7–15]. Due to the enormous difficulties of developing analytical descriptions for hydrogen plasmas with strong coupling, see for example [1–3], there is still an urgent need to test the analytical theory by an independent numerical approach.

An approach which is particularly well suited to the description of thermodynamic properties in the region of high pressure, characterized by strong coupling and strong

0741-3335/01/060743+17$30.00

degeneracy, is the path integral quantum Monte Carlo (PIMC) method. There has been remarkable recent progress in applying these techniques to Fermi systems, for an overview see for example [1, 2, 16–18]. However, these simulations are essentially hampered by the fermion sign problem. To overcome this difficulty, several strategies have been developed to simulate macroscopic Coulomb systems [8, 19, 20]: the first is the restricted PIMC concept where additional assumptions on the density operator $\hat{\rho}$ are introduced which reduce the sum over permutations to even (positive) contributions only. This requires knowledge of the nodes of the density matrix which is available only in a few special cases, see for example [19, 20]. However, for interacting macroscopic systems, these nodes are known only approximately (see e.g. [21]) and the accuracy of the results is difficult to assess from within this scheme [25]. An alternative are direct fermionic PIMC simulations, which have occasionally been attempted by various groups[4] but which were not sufficiently precise and efficient for practical purposes. Recently, three of us have proposed a new path integral representation for the N-particle density operator [23, 24] which allows for *direct fermionic path integral Monte Carlo* simulations of dense plasmas in a broad range of densities and temperatures. Using this concept we computed the pressure and energy of a degenerate strongly coupled hydrogen plasma [24, 26] and the pair distribution functions in the region of partial ionization and dissociation [26, 27]. This scheme is rather efficient when the number of time slices (beads) in the path integral is less than or equal to 50 and was found to work well for temperatures $k_{\mathrm{B}}T \gtrsim 0.1$ Ryd. In this paper we derive further improved formulae for the pressure and energy and give, for the first time, a detailed derivation of all main results and rigorously justify the use of the effective quantum pair potential (Kelbg potential) in direct PIMC simulations. Further, in the present work this method will be applied to high-pressure plasmas ($p \simeq 10^{-1}$–10^{2} Mbar) in such temperature regions were considerable deviations from the ideal behaviour are observed.

One difficulty of PIMC simulations is that reliable error estimates are often not available, in particular for strongly coupled degenerate systems. Moreover, in this region no reliable data from other theories such as density functional theory or quantum statistics (see e.g. [3, 15]) are available which would allow for an unambiguous test. Furthermore, results from classical molecular dynamics simulations exist, but they apply only to fully ionized and weakly degenerate plasmas (see e.g. [28–30]), which is outside the range of interest for this work. Also, new quantum molecular dynamics approaches are being developed (see e.g. [10–12]), but they are only beginning to produce accurate results.

Therefore, it is of high interest to perform quantitative comparisons of independent simulations, such as restricted and direct fermionic PIMC simulations, and to develop improved analytical approximations, which is the aim of this paper. We compare recent results of Militzer and Ceperley [31] for pressure and energy isochors ($n \sim 2.5 \times 10^{23}$ cm^{-3}) of dense hydrogen to our own direct PIMC results. This is a non-trivial comparison since the two approaches employ independent sets of approximations. Nevertheless, we find very good agreement for temperatures ranging from 10^{6} K to as low as 50 000 K. This is remarkable since there the coupling and degeneracy parameters reach rather large values, $\Gamma \approx 3$ and $n_{\mathrm{e}}\Lambda^{3} \approx 10$, and the plasma contains a substantial fraction of bound states.

Further, we use the new data to make a comparison with analytical estimates which are based on Padé approximations for strongly ionized plasmas. These formulae were constructed on the basis of the known analytical results for the limiting cases of low density [3, 32] and

[4] As an example we mention the method of Imada [22]. However, we have found that his approach is not adequate for thermodynamic properties. The method of Imada [22] ignores the sign of the exchange determinant, cf equation (19). We have found that Imada's approximation leads to essential errors for strongly degenerate systems. We underline that, in contrast, our method rigorously takes into account the sign of the determinant of each Monte Carlo configuration in the calculation of thermodynamic averages, such as pressure and energy, equations (17) and (20).

high density [3]. These Padé approximations are exact up to quadratic terms in the density and interpolate between the virial expansions and the high-density asymptotics [33–35]. We find that the results for the internal energy and for the pressure agree well with the PIMC results in the region of the density temperature plane, where $\Gamma \lesssim 1.6$ and $n\Lambda^3 \lesssim 5$.

2. Path integral representation of thermodynamic quantities

We now explain our direct PIMC scheme. All thermodynamic properties of a two-component plasma are defined by the partition function Z which, for the case of N_e electrons and N_p protons, is given by

$$Z(N_\mathrm{e}, N_\mathrm{p}, V, \beta) = \frac{Q(N_\mathrm{e}, N_\mathrm{p}, \beta)}{N_\mathrm{e}! N_\mathrm{p}!}$$

$$\text{with} \qquad Q(N_\mathrm{e}, N_\mathrm{p}, \beta) = \sum_\sigma \int_V \mathrm{d}q\, \mathrm{d}r\, \rho(q, r, \sigma; \beta) \tag{1}$$

where $\beta = 1/k_\mathrm{B}T$. The exact density matrix is, for a quantum system, in general, not known but can be constructed using a path integral representation [36],

$$\int_V \mathrm{d}R^{(0)} \sum_\sigma \rho(R^{(0)}, \sigma; \beta) = \int_V \mathrm{d}R^{(0)} \ldots \mathrm{d}R^{(n)}\, \rho^{(1)} \cdot \rho^{(2)} \ldots \rho^{(n)}$$
$$\times \sum_\sigma \sum_P (\pm 1)^{\kappa_P} \mathcal{S}(\sigma, \hat{P}\sigma') \hat{P} \rho^{(n+1)} \tag{2}$$

where $\rho^{(i)} \equiv \rho(R^{(i-1)}, R^{(i)}; \Delta\beta) \equiv \langle R^{(i-1)}|\mathrm{e}^{-\Delta\beta\hat{H}}|R^{(i)}\rangle$, whereas $\Delta\beta \equiv \beta/(n+1)$ and $\Delta\lambda_a^2 = 2\pi\hbar^2\Delta\beta/m_a$, $a = \mathrm{p}, \mathrm{e}$. $\hat{H}$ is the Hamilton operator, $\hat{H} = \hat{K} + \hat{U}_\mathrm{c}$, containing kinetic and potential energy contributions, $\hat{K}$ and $\hat{U}_\mathrm{c}$, respectively, with $\hat{U}_\mathrm{c} = \hat{U}_\mathrm{c}^\mathrm{p} + \hat{U}_\mathrm{c}^\mathrm{e} + \hat{U}_\mathrm{c}^\mathrm{ep}$ being the sum of the Coulomb potentials between protons (p), electrons (e) and electrons and protons (ep). Further, $R^{(i)} = (q^{(i)}, r^{(i)}) \equiv (R_\mathrm{p}^{(i)}, R_\mathrm{e}^{(i)})$, for $i = 1, \ldots, n+1$, $R^{(0)} \equiv (q, r) \equiv (R_\mathrm{p}^{(0)}, R_\mathrm{e}^{(0)})$, and $R^{(n+1)} \equiv R^{(0)}$ and $\sigma' = \sigma$. This means that the particles are represented by fermionic loops with the coordinates (beads) $[R] \equiv [R^{(0)}; R^{(1)}; \ldots; R^{(n)}; R^{(n+1)}]$, where q and r denote the electron and proton coordinates, respectively. The spin gives rise to the spin part of the density matrix $\mathcal{S}$, whereas exchange effects are accounted for by the permutation operator $\hat{P}$, which acts on the electron coordinates and spin projections, and the sum over the permutations with parity κ_P. In the fermionic case (minus sign), the sum contains $N_\mathrm{e}!/2$ positive and negative terms leading to the notorious sign problem. Due to the large mass difference of electrons and ions, the exchange of the latter is not included. The matrix elements $\rho^{(i)}$ can be rewritten identically as

$$\langle R^{(i-1)}|\mathrm{e}^{-\Delta\beta\hat{H}}|R^{(i)}\rangle = \int \mathrm{d}\tilde{p}^{(i)}\, \mathrm{d}\bar{p}^{(i)} \langle R^{(i-1)}|\mathrm{e}^{-\Delta\beta\hat{U}_\mathrm{c}}|\tilde{p}^{(i)}\rangle\langle\tilde{p}^{(i)}|$$
$$\times \mathrm{e}^{-\Delta\beta\hat{K}}|\bar{p}^{(i)}\rangle\langle\bar{p}^{(i)}|\mathrm{e}^{-\frac{\Delta\beta^2}{2}[\hat{K},\hat{U}_\mathrm{c}]} \ldots |R^{(i)}\rangle. \tag{3}$$

To compute thermodynamic functions, the logarithm of the partition function has to be differentiated with respect to thermodynamic variables. In particular, for the equation of state p and internal energy E,

$$\beta p = \partial \ln Q/\partial V = [\alpha/3V \partial \ln Q/\partial\alpha]_{\alpha=1} \tag{4}$$

$$\beta E = -\beta \partial \ln Q/\partial\beta \tag{5}$$

where α is a length scaling parameter $\alpha = L/L_0$. This means, in the path integral representation (2), each high-temperature density matrix has to be differentiated in turn.

For example, the result for the energy will have the form

$$\beta E = -\frac{1}{Q}\int_V \mathrm{d}R^{(0)}\ldots\mathrm{d}R^{(n)}\sum_{k=1}^{n+1}\rho^{(1)}\ldots\rho^{(k-1)}\cdot\left[\beta\frac{\partial\rho^{(k)}}{\partial\beta}\right] \cdot\rho^{(k+1)}\ldots\rho^{(n)}\sum_{\sigma}\sum_{P}(\pm1)^{\kappa_P}\mathcal{S}(\sigma,\hat{P}\sigma')\hat{P}\rho^{(n+1)} \tag{6}$$

and analogously for other thermodynamic functions.

There are two different approaches to evaluating this expression. One is to first choose an approximation for the high-temperature density matrices $\rho^{(i)}$ and then to perform the differentiation. The other way is to first differentiate the operator expression for $\rho^{(k)}$ and use an approximation for the matrix elements only in the final result. As we checked, the second method is more accurate and will be used in the following.

To evaluate the derivatives in equation (6), it is convenient to introduce dimensionless integration variables $\eta^{(k)} = (\eta_{\mathrm{p}}^{(k)}, \eta_{\mathrm{e}}^{(k)})$, where $\eta_a^{(k)} = \kappa_a(R_a^{(k)} - R_a^{(k-1)})$ for $k = 1,\ldots,n$ and $a = \mathrm{p},\mathrm{e}$, and $\kappa_a^2 \equiv m_a k_{\mathrm{B}}T/(2\pi\hbar^2) = 1/\lambda_a^2$ [24]. This has the advantage that now the differentiation of the density matrix affects only the interaction terms. Indeed, one can show that

$$\beta\frac{\partial\rho^{(k)}}{\partial\beta} = -\beta\frac{\partial\Delta\beta\cdot U_c(X^{(k-1)})}{\partial\beta}\rho^{(k)} + \beta\tilde{\rho}_\beta^{(k)} \tag{7}$$

where $X^{(0)} \equiv (\kappa_{\mathrm{p}}R_{\mathrm{p}}^{(0)}, \kappa_{\mathrm{e}}R_{\mathrm{e}}^{(0)})$, $X^{(k)} \equiv (X_{\mathrm{p}}^{(k)}, X_{\mathrm{e}}^{(k)})$, with $X_a^{(k)} = \kappa_a R_a^{(0)} + \sum_{l=1}^{k}\eta_a^{(l)}$, and k runs from 1 to n. Further, $X^{(n+1)} \equiv (\kappa_{\mathrm{p}}R_{\mathrm{p}}^{(n+1)}, \kappa_{\mathrm{e}}R_{\mathrm{e}}^{(n+1)}) = X^{(0)}$, and we denote

$$\tilde{\rho}_\beta^{(k)} = \int \mathrm{d}p^{(k)}\langle X^{(k-1)}|\mathrm{e}^{-\Delta\beta\hat{U}_{\mathrm{c}}}|p^{(k)}\rangle\exp\left[-\frac{\langle p^{(k)}|p^{(k)}\rangle}{4\pi(n+1)}\right]\langle p^{(k)}|\frac{\partial}{\partial\beta}\mathrm{e}^{-\frac{(\Delta\beta)^2}{2}[\hat{K},\hat{U}_{\mathrm{c}}]}\ldots|X^{(k)}\rangle \tag{8}$$

where $p_a^{(k)} = \tilde{p}_a^{(k)}/(\kappa_a\hbar)$, $p(k) \equiv (p_{\mathrm{p}}^{(k)}, p_{\mathrm{e}}^{(k)})$ and use has been made of equation (3). For $k = n+1$, we have

$$\beta\frac{\partial}{\partial\beta}\sum_{\sigma}\sum_{P}(\pm1)^{\kappa_P}\mathcal{S}(\sigma,\hat{P}\sigma')\hat{P}\rho^{(n+1)} = \sum_{\sigma}\sum_{P}(\pm1)^{\kappa_P}\mathcal{S}(\sigma,\hat{P}\sigma') \times\left\{-\beta\frac{\partial\Delta\beta\cdot U_{\mathrm{c}}(X^{(n)})}{\partial\beta}\hat{P}\rho^{(n+1)} + \hat{P}[\beta\tilde{\rho}_\beta^{(n+1)}]\right\}. \tag{9}$$

Further, $U_{\mathrm{c}}(X^{(k-1)}) \equiv U_{\mathrm{c}}^{(1)}(X^{(k-1)}) + U_{\mathrm{c}}^{(2)}(X^{(k-1)})$, with $U_{\mathrm{c}}^{(1)}$ and $U_{\mathrm{c}}^{(2)}$ denoting the interaction between identical and different particle species, respectively, $U_{\mathrm{c}}^{(1)}(X) = U_{\mathrm{c}}^{\mathrm{e}}(X) + U_{\mathrm{c}}^{\mathrm{p}}(X)$ and $U_{\mathrm{c}}^{(2)}(X) = U_{\mathrm{c}}^{\mathrm{ep}}(X)$.

Using these results and equation (6), we obtain for the energy

$$\beta E = \frac{3}{2}(N_{\mathrm{e}}+N_{\mathrm{p}}) - \frac{1}{Q}\frac{1}{\lambda_{\mathrm{p}}^{3N_{\mathrm{p}}}\lambda_{\mathrm{e}}^{3N_{\mathrm{e}}}}\int_V \mathrm{d}R^{(0)}\,\mathrm{d}\eta^{(1)}\ldots\mathrm{d}\eta^{(n)}\sum_{\sigma}\sum_{P}(\pm1)^{\kappa_P}\mathcal{S}(\sigma,\hat{P}\sigma') \times\left\{\sum_{k=1}^{n+1}\rho^{(1)}\ldots\rho^{(k-1)}\left[-\beta\frac{\partial\Delta\beta\cdot U_{\mathrm{c}}^{(1)}(X^{(k-1)})}{\partial\beta} -\beta\frac{\partial\Delta\beta\cdot U_{\mathrm{c}}^{(2)}(X^{(k-1)})}{\partial\beta} + \beta\tilde{\rho}_\beta^{(n+1)}\right]\rho^{(k)}\ldots\rho^{(n)}\hat{P}\rho^{(n+1)}\right\}\Bigg|_{X^{(n+1)}=X^{(0)},\sigma'=\sigma}. \tag{10}$$

This way, the derivative of the density matrix has been calculated, and we turn to the next point—to find approximations for the high-temperature density matrix.

3. High-temperature asymptotics of the density matrix in the Path integral approach. The Kelbg potential

In this section we derive an approximation for the high-temperature density matrix which is suitable for direct PIMC simulations. Further, we demonstrate that the proper choice of the effective quantum pair potential is given by the Kelbg potential. Following [16, 37, 38], we derive a modified representation for the density matrix. The main steps are as follows.

(1) The N-particle density matrix is expanded in terms of two-particle, three-particle, etc, contributions from which only the first, ρ_{ab}, is retained [16, 37, 38].
(2) In the high-temperature limit, ρ_{ab} factorizes into a kinetic (ρ_0) and an interaction term (ρ_U^{ab}), $\rho_{ab} \approx \rho_0 \rho_U^{ab}$, because it can be shown that [39, 40]

$$\mathrm{e}^{-\frac{(\Delta\beta)^2}{2}[\hat{K},\hat{U}_c]} = \hat{I} + \mathrm{O}\left(\frac{1}{(n+1)^2}\right) \tag{11}$$

where $\hat{I}$ is the unity operator. In this way we get the following representation for the two-particle density matrix,

$$\rho_{ab} = \left(\frac{(m_a m_b)^{3/2}}{(2\pi\hbar\beta)^3}\right) \exp\left[-\frac{m_a}{2\hbar^2\beta}(\boldsymbol{r}_a - \boldsymbol{r}'_a)^2\right] \exp\left[-\frac{m_b}{2\hbar^2\beta}(\boldsymbol{r}_b - \boldsymbol{r}'_b)^2\right] \exp[-\beta\Phi_{ab}] \tag{12}$$

where $\Phi_{ab}(\boldsymbol{r}_a, \boldsymbol{r}'_a, \boldsymbol{r}_b, \boldsymbol{r}'_b)$ is the off-diagonal two-particle effective potential.
(3) In the following, the off-diagonal matrix elements of the effective binary potentials will be approximated by the diagonal ones by taking the Kelbg potential at the centre coordinate, $\Phi^{ab}(r, r'; \Delta\beta) \approx \Phi^{ab}((r + r')/2; \Delta\beta)$.
(4) For the plasma parameter region of interest, the protons can be treated classically, and Φ^{ii} may be approximated by the Coulomb potential.

We will now comment on these steps in more detail. We calculated the effective potential by solving a Bloch equation by first-order perturbation theory. The method has been described in detail in [40]. This procedure defines an effective off-diagonal quantum pair potential for Coulomb systems, which depends on the interparticle distances $\boldsymbol{r}_{ab}, \boldsymbol{r}'_{ab}$. As a result of first-order perturbation theory we get explicitly

$$\Phi^{ab}(\boldsymbol{r}_{ab}, \boldsymbol{r}'_{ab}, \Delta\beta) \equiv e_a e_b \int_0^1 \frac{\mathrm{d}\alpha}{d_{ab}(\alpha)} \mathrm{erf}\left(\frac{d_{ab}(\alpha)}{2\lambda_{ab}\sqrt{\alpha(1-\alpha)}}\right) \tag{13}$$

where $d_{ab}(\alpha) = |\alpha\boldsymbol{r}_{ab} + (1-\alpha)\boldsymbol{r}'_{ab}|$, $\mathrm{erf}(x)$ is the error function

$$\mathrm{erf}(x) = \frac{2}{\sqrt{\pi}} \int_0^x \mathrm{d}t\, \mathrm{e}^{-t^2}$$

and $\lambda_{ab}^2 = \hbar^2\Delta\beta/2\mu_{ab}$ with $\mu_{ab}^{-1} = m_a^{-1} + m_b^{-1}$. It is interesting to note that a simple approximation of the complicated integral over α by the length of the interval multiplied with the integrand in the centre (Mittelwertsatz) leads us to the so-called KTR potential due to Klakow, Toepffer and Reinhard which (in the diagonal approximation) is often used in quasi-classical molecular dynamics simulations [10, 13]

$$\Phi^{ab}(\boldsymbol{r}_{ab}, \boldsymbol{r}'_{ab}, \Delta\beta) \equiv \frac{e_a e_b}{d_{ab}(1/2)} \mathrm{erf}\left(\frac{d_{ab}(1/2)}{\lambda_{ab}}\right). \tag{14}$$

In our direct PIMC calculations we used the full expression for the interaction potential, keeping the α-integration but, in order to save computer time, we approximated the two-particle

interaction potential by its diagonal elements. The diagonal element ($\boldsymbol{r}'_{ab} = \boldsymbol{r}_{ab}$) of Φ^{ab} is just the familiar Kelbg potential, given by (we will use the same notation for the potential)

$$\Phi^{ab}(|\boldsymbol{r}_{ab}|, \Delta\beta) \equiv \Phi^{ab}(\boldsymbol{r}_{ab}, \boldsymbol{r}_{ab}, \Delta\beta) = \frac{e_a e_b}{\lambda_{ab} x_{ab}}[1 - \mathrm{e}^{-x_{ab}^2} + \sqrt{\pi} x_{ab}(1 - \mathrm{erf}(x_{ab}))] \tag{15}$$

where $x_{ab} = |\boldsymbol{r}_{ab}|/\lambda_{ab}$, and we underline that the Kelbg potential is finite at zero distance. The error of the above approximations, for each of the high-temperature factors on the right-hand side of equation (2), is of the order of $1/(n+1)^2$.

With these approximations, we obtain the result

$$\rho^{(k)} = \rho_0^{(k)} \rho_U^{(k)} + \mathrm{O}[1/(n+1)^2]$$

where $\rho_0^{(k)}$ is the kinetic density matrix, while

$$\rho_U^{(k)} = \mathrm{e}^{-\Delta\beta U(X^{(k-1)})} \delta(X^{(k-1)} - X^{(k)})$$

where U denotes the following sum of Coulomb and Kelbg potentials,

$$U(X^{(k)}) = U_{\mathrm{c}}^{\mathrm{p}}(X_{\mathrm{p}}^{(k)}) + U^{\mathrm{e}}(X_{\mathrm{e}}^{(k)}) + U^{\mathrm{ep}}(X_{\mathrm{p}}^{(k)}, X_{\mathrm{e}}^{(k)}).$$

Notice that special care has to be taken in performing the derivatives with respect to β of the Coulomb potentials which appear in equation (10). Indeed, products

$$\rho^{(1)} \ldots \rho^{(n)} \hat{P} \rho^{(n+1)} \beta \frac{\partial \Delta\beta \cdot U_{\mathrm{c}}(X^{(k-1)})}{\partial\beta}$$

have a singularity at zero interparticle distance which is integrable but leads to difficulties in the simulations. Due to the Kelbg potential, for the e–e and p–p interactions, this singularity is weakenend, but it is enhanced for the e–p interaction. In order to assure efficient simulations we, therefore, further transform the e–p contribution in the following way:

$$\begin{aligned}\int_0^1 \mathrm{d}\alpha \int \mathrm{d}R^{(k-1)} \langle R^{(k-2)}|\mathrm{e}^{-\Delta\beta\alpha\hat{K}}|R^{(k-1)}\rangle \Big[-\beta \frac{\partial}{\partial\beta}(\Delta\beta U_{\mathrm{c}}^{(2)}(R^{(k-1)}))\Big] \\ \times \langle R^{(k-1)}|\mathrm{e}^{-\Delta\beta(1-\alpha)\hat{K}}|R^{(k)}\rangle \\ \approx \langle R^{(k-1)}|\mathrm{e}^{-\Delta\beta\hat{K}}|R^{(k)}\rangle \Big[-\beta \frac{\partial}{\partial\beta}(\Delta\beta U^{(2)}(R^{(k-1)}))\Big] + \mathrm{O}[1/(n+1)^2].\end{aligned} \tag{16}$$

This means, within the standard error of our approximation $\mathrm{O}[(\Delta\beta)^2]$, we have replaced the e–p Coulomb potential $U_{\mathrm{c}}^{(2)}$ by the corresponding Kelbg potential $U^{(2)}$, which is much better suited for MC simulations.

Thus, using $\lambda_{\mathrm{p}} \ll \lambda_{\mathrm{e}}$, we finally obtain for the energy

$$\begin{aligned}\beta E = \frac{3}{2}(N_{\mathrm{e}} + N_{\mathrm{p}}) + \frac{1}{Q} \frac{1}{\lambda_{\mathrm{p}}^{3N_{\mathrm{p}}} \Delta\lambda_{\mathrm{e}}^{3N_{\mathrm{e}}}} \sum_{s=0}^{N_{\mathrm{e}}} \int \mathrm{d}q\, \mathrm{d}r\, \mathrm{d}\xi\, \rho_s(q, [r], \beta) \\ \times \Bigg\{ \sum_{p<t}^{N_{\mathrm{p}}} \frac{\beta\mathrm{e}^2}{|q_{pt}|} + \sum_{l=0}^{n} \Bigg[\sum_{p<t}^{N_{\mathrm{e}}} \frac{\Delta\beta\mathrm{e}^2}{|r_{pt}^l|} + \sum_{p=1}^{N_{\mathrm{p}}} \sum_{t=1}^{N_{\mathrm{e}}} \Psi_l^{\mathrm{ep}} \Bigg] \\ + \sum_{l=1}^{n} \Bigg[-\sum_{p<t}^{N_{\mathrm{e}}} C_{pt}^l \frac{\Delta\beta\mathrm{e}^2}{|r_{pt}^l|^2} + \sum_{p=1}^{N_{\mathrm{p}}} \sum_{t=1}^{N_{\mathrm{e}}} D_{pt}^l \frac{\partial \Delta\beta \Phi^{\mathrm{ep}}}{\partial |x_{pt}^l|} \Bigg] \\ - \frac{1}{\det|\psi_{ab}^{n,1}|_s} \frac{\partial \det|\psi_{ab}^{n,1}|_s}{\partial\beta} \Bigg\}\end{aligned}$$

$$\text{with} \qquad C_{pt}^l = \frac{\langle r_{pt}^l | y_{pt}^l \rangle}{2|r_{pt}^l|} \qquad D_{pt}^l = \frac{\langle x_{pt}^l | y_{\mathrm{p}}^l \rangle}{2|x_{pt}^l|} \tag{17}$$

and $\Psi_l^{\rm ep} \equiv \Delta\beta\partial[\beta'\Phi^{\rm ep}(|x_{pt}^l|,\beta')]/\partial\beta'|_{\beta'=\Delta\beta}$ contains the electron–proton Kelbg potential $\Phi^{\rm ep}$. Here, $\langle\ldots|\ldots\rangle$ denotes the scalar product, and q_{pt}, r_{pt} and x_{pt} are differences of two coordinate vectors: $q_{pt} \equiv q_{\rm p} - q_t$, $r_{pt} \equiv r_{\rm p} - r_t$, $x_{pt} \equiv r_{\rm p} - q_t$, $r_{pt}^l = r_{pt} + y_{pt}^l$, $x_{pt}^l \equiv x_{pt} + y_{\rm p}^l$ and $y_{pt}^l \equiv y_{\rm p}^l - y_t^l$, with $y_a^n = \Delta\lambda_{\rm e}\sum_{k=1}^n \xi_a^{(k)}$. Here we have introduced dimensionless distances between neighbouring vertices on the loop, $\xi^{(1)},\ldots,\xi^{(n)}$, thus, explicitly, $[r] \equiv [r; y_{\rm e}^{(1)}; y_{\rm e}^{(2)}; \ldots]$. Further, the density matrix ρ_s in equation (17) is given by

$$\rho_s(q,[r],\beta) = C_{N_{\rm e}}^s\, {\rm e}^{-\beta U(q,[r],\beta)} \prod_{l=1}^{n}\prod_{p=1}^{N_{\rm e}} \phi_{pp}^l \det|\psi_{ab}^{n,1}|_s \tag{18}$$

where $U(q,[r],\beta) = U_{\rm c}^{\rm p}(q) + \{U^{\rm e}([r],\Delta\beta) + U^{\rm ep}(q,[r],\Delta\beta)\}/(n+1)$ and $\phi_{\rm pp}^l \equiv \exp[-\pi|\xi_{\rm p}^{(l)}|^2]$. We underline that the density matrix (18) does not contain an explicit sum over the permutations and thus no sum of terms with alternating sign. Instead, the whole exchange problem is contained in a single exchange matrix given by

$$\|\psi_{ab}^{n,1}\|_s \equiv \left\| \exp\left[-\frac{\pi}{\Delta\lambda_{\rm e}^2}|(r_a - r_b) + y_a^n|^2 \right]_s \right\|. \tag{19}$$

As a result of the spin summation, the matrix carries a subscript s denoting the number of electrons having the same spin projection. For more details, we refer to [23, 24].

In similar way, we obtain the result for the equation of state,

$$\begin{aligned}
\frac{\beta pV}{N_{\rm e}+N_{\rm p}} = 1 + \frac{1}{N_{\rm e}+N_{\rm p}} \frac{(3Q)^{-1}}{\lambda_{\rm p}^{3N_{\rm p}}\Delta\lambda_{\rm e}^{3N_{\rm e}}} \sum_{s=0}^{N_{\rm e}} \int {\rm d}q\,{\rm d}r\,{\rm d}\xi\; \rho_s(q,[r],\beta) \\
\times\Bigg\{ \sum_{p<t}^{N_{\rm p}} \frac{\beta e^2}{|q_{pt}|} + \sum_{p<t}^{N_{\rm e}} \frac{\Delta\beta e^2}{|r_{pt}|} - \sum_{p=1}^{N_{\rm p}}\sum_{t=1}^{N_{\rm e}} |x_{pt}| \frac{\partial\,\Delta\beta\Phi^{\rm ep}}{\partial|x_{pt}|} \\
+ \sum_{l=1}^{n}\Bigg[\sum_{p<t}^{N_{\rm e}} A_{pt}^l \frac{\Delta\beta e^2}{|r_{pt}^l|^2} - \sum_{p=1}^{N_{\rm p}}\sum_{t=1}^{N_{\rm e}} B_{pt}^l \frac{\partial\,\Delta\beta\Phi^{\rm ep}}{\partial|x_{pt}^l|}\Bigg] \\
+ \frac{\alpha}{\det|\psi_{ab}^{n,1}|_s} \frac{\partial \det|\psi_{ab}^{n,1}|_s}{\partial\alpha} \Bigg\} \\
\text{with} \qquad A_{pt}^l = \frac{\langle r_{pt}^l | r_{pt}\rangle}{|r_{pt}^l|} \qquad\qquad B_{pt}^l = \frac{\langle x_{pt}^l | x_{pt}\rangle}{|x_{pt}^l|}.
\end{aligned} \tag{20}$$

The structure of equations (17) and (20) is obvious: we have separated the classical ideal gas part (first term). The ideal quantum part in excess of the classical one and the correlation contributions are contained in the integral term, where the second line results from the ionic correlations (first term) and the e–e and e–i interaction at the first vertex (second and third terms, respectively). The third and fourth lines are due to the further electronic vertices and the explicit temperature dependence (in equation (17) and volume dependence in equation (20)) of the exchange matrix, respectively. The main advantage of equations (17) and (20) is that the explicit sum over permutations has been converted into the spin determinant which can be computed very efficiently using standard linear algebra methods. Furthermore, each of the sums in curly brackets in equations (17) and (20) is bounded as the number of vertices increases, $n \to \infty$, and is thus well suited for efficient Monte Carlo simulations. Notice also that equations (17) and (20) contain the important limit of an ideal quantum plasma in a natural way[5].

[5] An energy estimator similar to equation (17) has been derived by Herman *et al* [41] but their result neglects the spin statistics and does not contain the correct non-interacting limit.

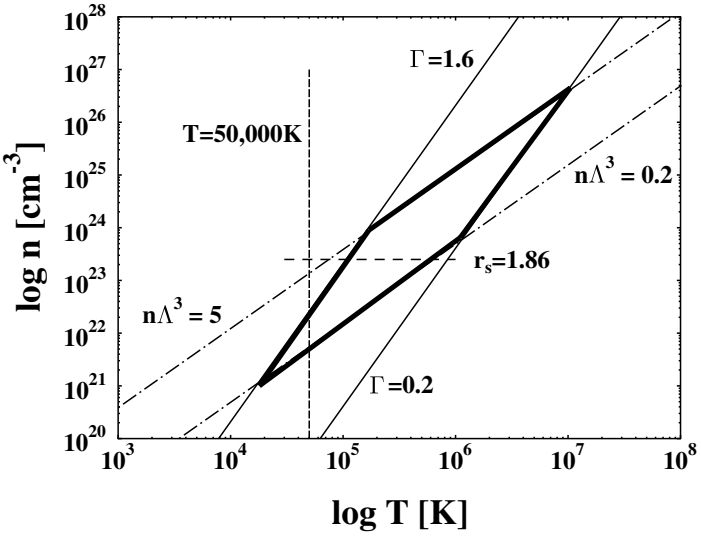

Figure 1. Density–temperature plane showing the parameter region for which calculations are performed. The data of figure 2 are along the dashed line (isochor $r_s = 1.86$). The data of figures 3 and 4 are inside the bold rhombus, along lines of constant Γ between the lines $n\Lambda^3 = 0.2$ and $n\Lambda^3 = 5$, respectively. Data for the vertical line (isotherm $T = 50\,000$ K) are given in figure 5.

4. Comparison of direct and restricted PIMC simulations

Expressions (17) and (20) are well suited for numerical evaluation using Monte Carlo techniques, see for example [16, 17]. In our Monte Carlo scheme we used three types of steps, where either electron or proton coordinates, r_i or q_i, or individual electronic beads $\xi_i^{(k)}$ were moved until convergence of the calculated values was reached. Our procedure has been extensively tested. In particular, we found from comparison with the known analytical expressions for pressure and energy of an ideal Fermi gas that the Fermi statistics is very well reproduced [26]. Further, we performed extensive tests for few-electron systems in a harmonic trap where, again, the analytically known limiting behaviour (e.g. energies) is well reproduced [42, 43]. For the present simulations of dense hydrogen, we varied both the particle number and the number of time slices (beads). As a result of these tests, we found that to obtain convergent results for the thermodynamic properties of dense hydrogen, particle numbers $N_e = N_p = 50$ and beads numbers in the range $n = 6 \ldots 20$ are adequate [24, 26].

We will now compare our results with some available results obtained by the Monte Carlo technique developed by the Urbana group [19, 31]. We may first state that both Monte Carlo techniques differ in several fundamental points, so that they are essentially independent approaches. Let us briefly outline the main differences between the technique developed in Urbana, known as the *restricted PIMC* scheme, cf [31] and references therein, and the approach described here. The authors of [31] performed simulations with 32 electrons and protons; their restricted PIMC scheme required the use of a rather small time step assuring $1/\Delta\beta \sim 2\times 10^6$ K. Also, their treatment of the interactions differs from our scheme: the authors of [31] perform a numerical solution of the Bloch equation for the two-particle density matrix whereas we use an analytical approximation for the effective pair interaction (based on the Kelbg potential, see above). Finally, [31] approximately computes the nodal surface of the density matrix using a variational ansatz which is then used to restrict the integrations to the region of positive density matrix. For more details regarding the restricted PIMC simulations, see [19, 31].

Let us now turn to a comparison of the numerical results. The restricted PIMC simulation data for dense hydrogen are taken from [31]. A comparison of results for the pressure and the internal energy for a fixed value of the density ($r_s = 1.86$) is shown in figure 1 and table 1. At high temperatures, above 50 000 K, where only a small fraction of atoms is expected, the agreement is rather good. This is remarkable since the non-ideality and the degeneracy reach values of 3 and 10, respectively. This result demonstrates that, at least for $r_s \simeq 1$ and for $T \geqslant 50\,000$ K, both methods yield results which are more or less equivalent. At $T < 50\,000$ K, where partial ionization is expected, we still observe a reasonable agreement of both approaches; however, we see also that the differences start to grow. The reasons for this are manyfold. From our results we conclude that the main problem is not the bound-state formation—atoms and molecules are well described by the two PIMC simulations which use a physical picture which does not involve any artificial distinction between free and bound electrons, see for example [26]. On the other hand, with growing degeneracy $n\Lambda^3$, both PIMC methods become less reliable, and a detailed analysis, although being very desirable, will have to be based on more extensive calculations in the future [25].

Table 1. Direct versus restricted PIMC [23] simulation results (upper and middle lines, respectively) and results of Padé calculations (numbers in the lowest lines) for the pressure p (Mbar) and energy E (2NRy) for dense hydrogen (deuterium [23]) for $r_s = 1.86$.

T (1000 K)	$n\Lambda^3$	Γ	p (Mbar)	E (2NRy)
1000	0.10	0.169	67.74 ± 0.02	9.050 ± 0.005
			66.86 ± 0.08	9.018 ± 0.015
			67.38	9.063
500	0.29	0.339	32.85 ± 0.03	4.169 ± 0.003
			32.13 ± 0.05	4.114 ± 0.007
			31.91	4.162
250	0.83	0.679	15.37 ± 0.01	1.654 ± 0.005
			14.91 ± 0.03	1.629 ± 0.007
			14.40	1.679
125	2.33	1.350	6.98 ± 0.01	0.412 ± 0.005
			6.66 ± 0.02	0.404 ± 0.004
			6.47	0.471
62.5	6.58	2.701	3.07 ± 0.02	-0.248 ± 0.005
			2.99 ± 0.04	-0.140 ± 0.007
31.25	18.48	5.376	2.20 ± 0.01	-2.377 ± 0.005
			1.58 ± 0.07	-0.360 ± 0.010

Further we also present in table 1 Padé results for the weakly non-ideal region. We find good agreement with the PIMC results for $T > 10^5$ K. Details on the method of these analytical calculations will be discussed in the next section.

5. Comparison with analytical approximations for the thermodynamic functions of strongly ionized dense plasmas

In this section we give a comparison of the available data points from direct PIMC calculations with analytical estimates based on Padé approximations for strongly ionized plasmas [3, 33–35]. The comparison concentrates on H-plasmas in a region in the density–temperature plane with the following borders

$$0.2 \leqslant \Gamma \leqslant 1.6 \qquad 0.2 \leqslant n_e \Lambda_e^3 \leqslant 5 \tag{21}$$

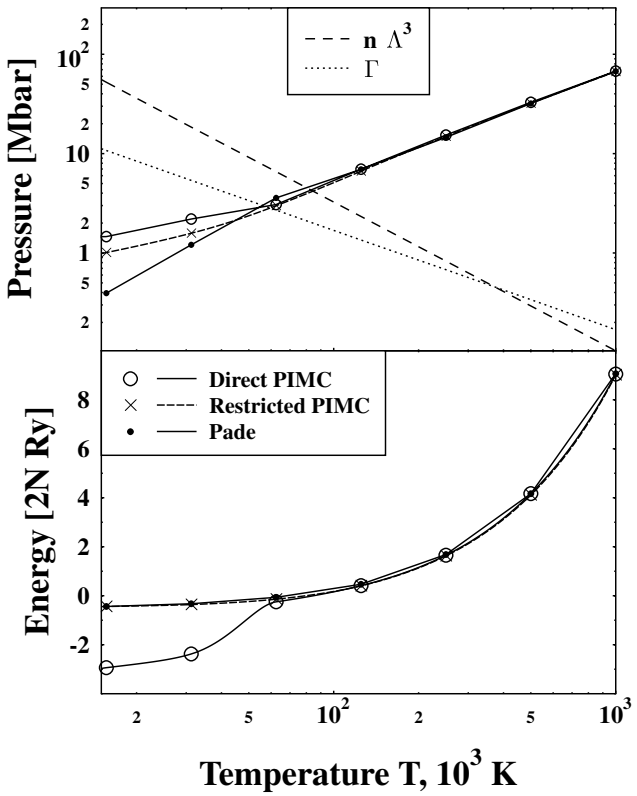

Figure 2. Comparison of direct and restricted PIMC results and analytical results (Padé) for the pressure and total energy of dense hydrogen as a function of temperature for $r_s = 1.86$, corresponding to $n = 2.5 \times 10^{23}$ cm^{-3}. For illustration, the coupling and degeneracy parameters Γ and $n_e\Lambda^3$ are also shown in the upper figure.

which will be called 'rhombus of moderate non-ideality and moderate degeneracy' (see the bold rhombus in figure 1). With respect to the analytical treatment, this rhombic region is of particular difficulty since none of the known analytic limiting expressions are valid. Further, we calculated several points for $r_s = 1.86$ and $\Gamma \lesssim 2$ which correspond to the PIMC data discussed in the previous section and also an isotherm at $T = 50\,000$ K, including some data at higher density outside the rhombus, cf figure 1 for an overview.

We demonstrate below that the Padé approximations which interpolate between the limits where theoretical results are available are a useful tool for the description of the available data points, at least for the case of moderate non-ideality $\Gamma \lesssim 1.6$ and moderate degeneracy $n_e\Lambda^3 \lesssim 5$. The Padé approximations which we use here were constructed in earlier work [33, 35] from the known analytical results for limiting cases of low density [3, 32] and high density [3]. The structure of the Padé approximations was devised in such a way that they are analytically exact up to quadratic terms in the density (up to the second virial coefficient) and interpolate between the virial expansions and the high-density asymptotic expressions [33–35]. The formation of bound states was taken into account by using a chemical picture. This means the plasma is considered as a mixture of free electrons, free ions, atoms and molecules which are in chemical equilibrium, being described by mass action laws or minimization of the free energy [35].

We follow to a large part this cited work here, with only the contribution of the ion–ion interaction, which is, in most cases, the largest one, being substantially improved following a recent work of Kahlbaum, who succeeded in describing the available classical Monte Carlo data for the ions by accurate Padé approximations [45]. By using Kahlbaum's formulae we achieve a rather accurate description of the thermodynamics in the region where the plasma behaves like a classical one-component plasma (OCP) of ions embedded into a sea of nearly ideal electrons. This is the region where the electrons are strongly degenerate,

$$n_e \Lambda_e^3 \gg 1 \qquad \text{and} \qquad r_s \ll 1 \tag{22}$$

and the ions are still classical but non-ideal,

$$\Gamma \gg 1 \qquad \text{and} \qquad n_i \Lambda_i^3 \ll 1. \tag{23}$$

This region lies in the upper left corner of figure 1.

With respect to the chemical picture we restrict ourselves to the region of strong ionization where the number of atoms is still relatively low and where the fraction of molecules is small as well, see below. We will discuss here only the general structure of the Padé formulae. For example, the internal energy density of the plasma is given by

$$u = u_{id} + u_{int}. \tag{24}$$

Here u_{id} is the internal energy of an ideal plasma consisting of Fermi electrons, classical protons and classical atoms, and u_{int} is the interaction energy

$$u_{int} = u_{ii} + u_{ee} + u_{ie} + u_{vdW}. \tag{25}$$

The interaction contribution to the internal energy consists of four terms.

- *Ion–ion interaction contribution*: this term which, in general, yields the largest contribution is generated by the OCP subsystem of the protons. For the OCP energy of protons many expressions are available, see for example [44]. We have used here the most precise formula due to Kahlbaum [45] which interpolates between the Debye region, $u_{ii} \sim \Gamma^{3/2}$, and the high density fluid, $u_{ii} \sim \Gamma$.
- *Electron–electron interaction*: This term corresponds to the OCP energy of the electron subsystem. We used the rather simple expressions used in earlier work [33, 34].
- *Electron–proton interaction*: This term corresponds to the interaction between the two OCP subsystems which is mostly due to polarization effects. Again, we used the rather simple expressions proposed in earlier work [33, 34].
- *Van der Waals contribution*: In the region of densities and temperatures defined above this contribution gives only a small correction. Therefore, this term was approximated here in the simplest way by a second virial contribution. The neutral particles were treated as hard spheres.

In the region of densities which are studied here, molecules do not play a role; therefore, the formation of molecules was taken into account only in a very rough approximation according to [33]. The number density of the neutrals was calculated on the basis of a non-ideal Saha equation. We restricted this comparison to a region where the number density of neutrals is relatively small, the degree of ionization being larger than 75%.

The contributions to the pressure were calculated, in part, from scaling relations, for example we used $p_{ii} = u_{ii}/3$, and, for the other (smaller) contributions, by numerical differentiation of the free energy given earlier [33, 34]. In a similar way, the chemical potential which appears in the non-ideal Saha equation was obtained. For the partition function in the Saha equation we used the Brillouin–Planck–Larkin expression [3, 35]. The solution of the non-ideal Saha equation which determines the degree of ionization (the

density of the atoms) was solved by up to 100 iterations starting from the ideal Saha equation.

Since all the expressions described so far are given in analytic form, the calculation of about 1000 data points for energy and pressure takes less than a minute on a PC. The result of our calculations for density–temperature points in the 'rhombus of moderate non-ideality and moderate degeneracy' are given in figures 3 and 4. Further, we include in table 1 several data points obtained from the Padé formulae. (Since the Padé formulae used here do not apply to low temperatures, we included only Padé data for $T > 10^5$ K.)

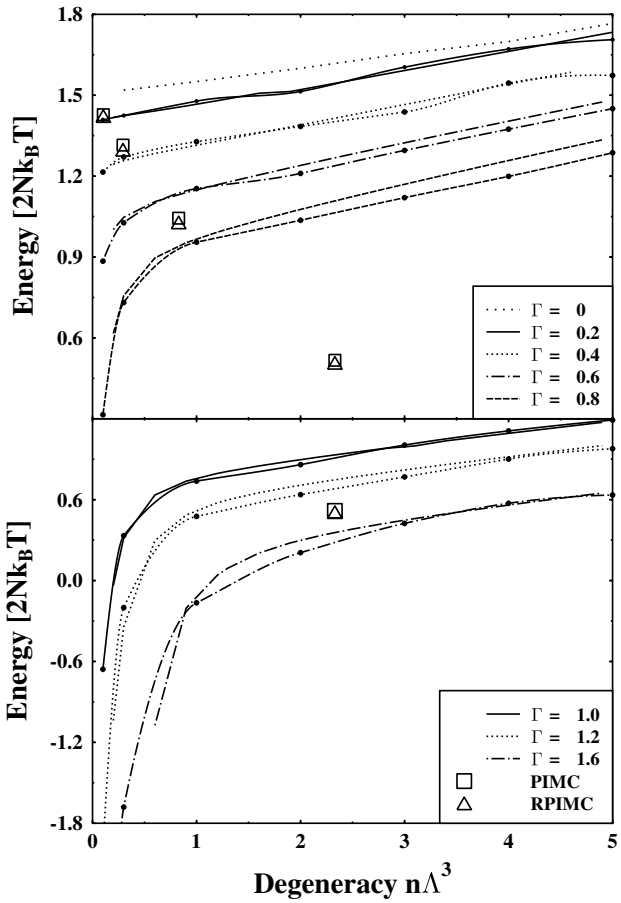

Figure 3. Comparison of Padé calculations (curves without symbols) for the internal energy with the direct PIMC results (curves with full circles). Triangles and squares show the level of agreement between restricted and direct PIMC (denoted RPIMC and PIMC, respectively) in this parameter region (Γ values differ from those of the lines).

Summarizing the results for the internal energy and for the pressure, we find that the Padé results, with a few exceptions, agree well with the PIMC data in the region of the density temperature plane, where $\Gamma \leqslant 1.6$ and $n\Lambda^3 \leqslant 5$. The agreement is particularly good for the energies. (The larger deviations for the pressure may be due to the numerical differentiation.) In fact, the Padé formulae used here in combination with the chemical picture work only in the case when the plasma is strongly ionized, i.e. the degree of ionization is larger than 75%.

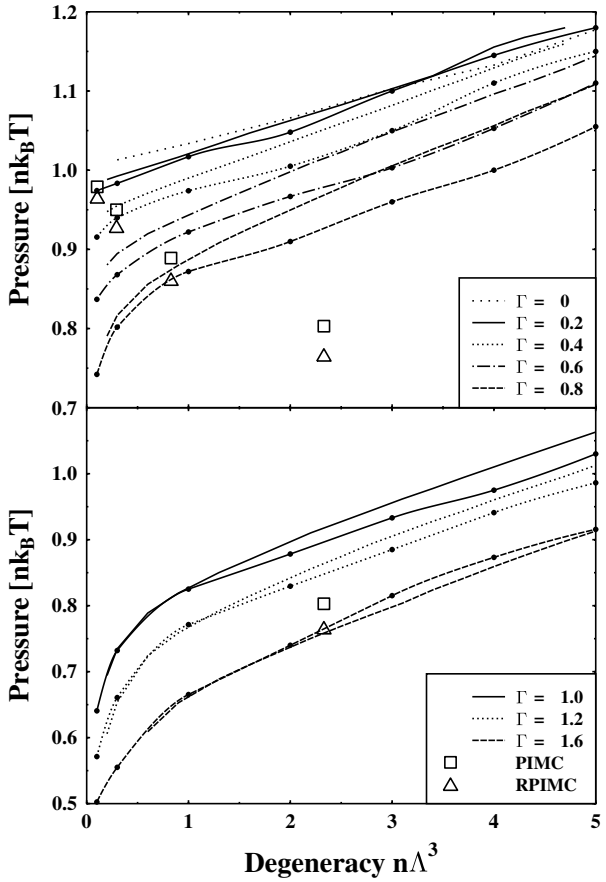

Figure 4. Comparison of Padé calculations (curves without symbols) of the pressure (in units of the Boltzmann pressure) with direct PIMC simulation results (curves with full circles). Triangles and squares show the level of agreement between restricted and direct PIMC (denoted RPIMC and PIMC, respectively) in this parameter region (Γ values differ from those of the lines).

The description of the region where a higher percentage of atoms and, due to this, also molecules is present needs a more refined chemical picture [7, 46, 47].

Finally, we compare the Padé and PIMC data along the isotherm $T = 50\,000$ K which is given in figure 5. This figure shows the transition from a classical ideal gas (low density) to a nearly ideal quantum gas (limit of high density). In the central part, $n \lesssim 10^{19}$ cm$^{-3} \lesssim 10^{25}$ cm^{-3}, the Coulomb interaction leads to strong deviations from the behaviour of an ideal plasma. The strong increase of the energy at high density is due to the Mott effect and to the increase of the ideal quantum contribution to the electron energy. Comparing the Padé and PIMC results, we find good agreement up to electron densities $n = 10^{22}$ cm^3. For higher densities, the deviations are growing. For intermediate densities, $n \lesssim 10^{22}$ cm$^{-3} \lesssim 10^{24}$ cm^{-3}, the PIMC data are more reliable. On the other hand, in the limit of very high density, $r_s \ll 1$, the Padé results are known to correctly approach the ideal quantum plasma limit whereas the PIMC data should be regarded as preliminary due to the extremely high electron degeneracy. Interestingly, we find that at high density the Padé data approach the ideal curves earlier than the PIMC data which is important for further improvement of the presented Monte Carlo approach.

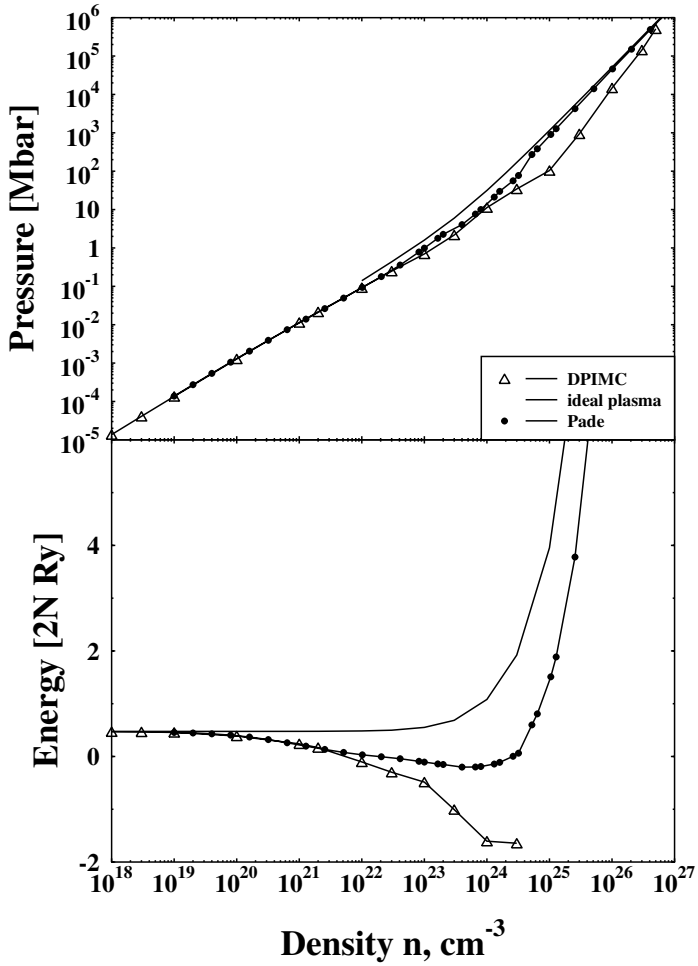

Figure 5. Comparison of Padé calculations (curves without symbols) of the pressure (in units of the Boltzmann pressure) with direct PIMC simulation results (curves with full circles) for the isotherm $T = 50\,000$ K.

6. Discussion

This work is devoted to the investigation of the thermodynamic properties of hot dense partially ionized plasmas in the pressure range between 0.1 and 100 Mbar. Most of the new results are based on a quantum Monte Carlo study of a correlated proton–electron system with degenerate electrons and classical protons. In this paper, we have given a detailed derivation of improved estimators for the internal energy and the equation of state for use in direct fermionic path integral simulations. Also, we have given a rigorous justification for the use of an effective quantum pair potential (Kelbg potential) in PIMC simulations.

Further, we have compared our direct PIMC results with the independent restricted PIMC data of Militzer and Ceperley for one isochor corresponding to $r_s = 1.86$, see figure 2. We found very good quantitative agreement between the two PIMC methods for temperatures in the range of $50\,000$ K $\leqslant T \leqslant 10^6$ K, where $\Gamma \lesssim 3$ and $n_e\Lambda_e^3 \lesssim 10$. This

region is particularly complicated as here pressure and temperature ionization occur here and, therefore, an accurate and consistent treatment of scattering and bound states is crucial. This agreement is remarkable because the two simulation methods are completely independent and use essentially different approximations. We, therefore, expect that the results for the thermodynamic properties of high-pressure hydrogen plasmas in this temperature–density range are reliable within the limits of the simulation accuracy. This is the main result of the present paper.

In future work, it will be important to extend the range of agreement. To analyse the deviations between the two simulation methods, we also included some data for $r_s = 1.86$ and lower temperatures, $10\,000\ \mathrm{K} \leqslant T \leqslant 50\,000$ K, see figure 2. At this point, no conclusive answer about the reasons for the deviations can be given. For these parameters, the electron degeneracy grows rapidly and, therefore, each of the simulation methods becomes less reliable. So these data should be regarded as preliminary results which will be useful for future improvements of the simulations.

Furthermore, the Monte Carlo results have allowed us to develop and test analytical approximations of Padé type which are improvements of earlier approximations [3, 33–35] in a region in the density–temperature plane bounded by $\Gamma \leqslant 1.6$ and $n_e \Lambda_e^3 \leqslant 5$. This is a region of *moderate non-ideality and degeneracy and high degree of ionization*. We have shown that, for these parameters, the Padé approximations which interpolate between the limits where theoretical results are available agree well with the Monte Carlo data, cf figures 2–4 and table 1. Thus, these approximations provide a useful tool for the description of these plasmas which include hydrogen at a pressure between 0.1 and 100 Mbar. At lower temperatures, deviations from the Monte Carlo data grow, cf figure 2. This is mostly due to the growing role of bound states. Whether the Padé approximations, in combination with an improved chemical picture (mass action law), continue to work at lower temperatures has still to be explored; the first steps are under way [47].

Also, we have shown some data for $T = 50\,000$ K and higher pressure, up to $p \sim 10^6$ Mbar, see figure 5. Here the Monte Carlo simulations are particularly difficult due to the high electron degeneracy, and they can benefit from the Pade simulations, as the latter correctly reproduce the high-density limit, $r_s \ll 1$.

Acknowledgments

We acknowledge stimulating discussions with W D Kraeft, D Kremp and M Schlanges. We thank D M Ceperley and B Militzer for discussions on PIMC concepts and for providing us with the data of [31] prior to publication. Further we thank J Ortner for informing us about an alternative derivation for the off-diagonal elements of the interaction potential. This work was made possible by generous support from the Deutsche Forschungsgemeinschaft (Mercator-Programm and grant BO-1366/2) and by a grant for CPU time at the NIC Jülich.

References

[1] Kalman G (ed) 1998 *Strongly Coupled Coulomb Systems* (Oxford: Pergamon)
[2] Kraeft W D and Schlanges M (eds) 1996 *Proc. Int. Conf. on Strongly Coupled Plasmas* (Singapore: World Scientific)
[3] Kraeft W D, Kremp D, Ebeling W and Röpke G 1986 *Quantum Statistics of Charged Particle Systems* (Berlin: Akademie)
[4] Bonitz M (ed) 2000 *Progress in Nonequilibrium Green's Functions* (Singapore: World Scientific)
[5] Ebeling W, Förster A, Hess H and Romanovsky M Yu 1996 *Plasma Phys. Control. Fusion* **38** A31–A47

[6] Da Silva I B *et al* 1997 *Phys. Rev. Lett.* **78** 783
[7] Schlanges M, Bonitz M and Tschttschjan A 1995 *Contrib. Plasma Phys.* **35** 109
[8] For completeness, we mention interesting attempts to overcome the fermion sign problem in path integral Monte Carlo simulations for *few-electron* systems by appropriately regrouping the sum over permutations, cf Egger R, Häusler W, Mak C H and Grabert H 1999 *Phys. Rev. Lett.* **82** 3320 and references therein
[9] Ebeling W, Stolzmann W, Förster A and Kasch M 1999 *Contrib. Plasma Phys.* **39** 287
[10] Klakow D, Toepffer C and Reinhard P-G 1994 *Phys. Lett.* A **192** 55
Klakow D, Toepffer C and Reinhard P-G 1994 *J. Chem. Phys.* **101** 10 766
[11] Knaup M *et al* 2000 *J. Physique* IV **10** 307
[12] Filinov V S, Levashov P R, Fortov V E and Bonitz M 2000 *J. Physique* IV **10** 323
[13] Ebeling W and Schautz F 1997 *Phys. Rev.* E **56** 3498
[14] Bonitz M *et al* 1996 *J. Phys.: Condens. Matter* **8** 6057
[15] Bonitz M 1998 *Quantum Kinetic Theory* (Stuttgart/Leipzig: Teubner)
[16] Zamalin V M, Norman G E and Filinov V S 1977 *The Monte Carlo Method in Statistical Thermodynamics* (Moscow: Nauka) (in Russian)
[17] Binder K and Cicotti G (eds) 1996 *The Monte Carlo and Molecular Dynamics of Condensed Matter Systems* (Bologna: SIF)
[18] Berne B J, Ciccotti G and Coker D F (eds) 1998 *Classical and Quantum Dynamics of Condensed Phase Simulation* (Singapore: World Scientific)
[19] Ceperley D M 1996 *The Monte Carlo and Molecular Dynamics of Condensed Matter Systems* ed K Binder and G Cicotti (Bologna: SIF) pp 447–82
[20] Ceperley D M 1995 *Rev. Mod. Phys.* **65** 279
[21] Militzer B and Pollock R 2000 *Phys. Rev.* E **61** 3470
[22] Imada 1984 *J. Phys. Soc. Japan* **53** 2861
[23] Filinov V S, Levashov P R, Fortov V E and Bonitz M 2000 *Progress in Nonequilibrium Green's Functions* ed M Bonitz (Singapore: World Scientific)
[24] Filinov V S and Bonitz M *Preprint* cond-mat/9912049
[25] Filinov V S 2001 *J. Phys. A: Math. Gen.* **34** 1665
[26] Filinov V S, Bonitz M and Fortov V E 2000 *JETP Lett.* **72** 245
[27] Filinov V S, Fortov V E, Bonitz M and Kremp D 2000 *Phys. Lett.* A **274** 228
[28] Zwicknagel G, Toepffer C and Reinhard P-G 1999 *Phys. Rep.* **314** 671
[29] Golubnychiy V, Bonitz M, Kremp D and Schlanges M *Phys. Rev.* E, at press
[30] Golubnychiy V, Bonitz M, Kremp D and Schlanges M 2001 *Contrib. Plasma Phys.*
[31] Militzer B and Ceperley D M 2000 *Phys. Rev. Lett.* **85** 1890
[32] Ebeling W 1968 *Ann. Phys., Lpz.* **21** 315
Ebeling W 1969 *Ann. Phys., Lpz.* **22** 33
Ebeling W 1969 *Ann. Phys., Lpz.* **22** 383
Ebeling W 1969 *Ann. Phys., Lpz.* **22** 392
Ebeling W 1968 *Physica* **38** 378
Ebeling W 1968 *Physica* **40** 290
[33] Ebeling W and Richert W 1985 *Phys. Lett.* A **7108** 80
Ebeling W and Richert W 1985 *Phys. Status Solidi* b **128** 167
[34] Ebeling W 1989 *Contrib. Plasma Phys.* **29** 165
Ebeling W 1990 *Contrib. Plasma Phys.* **30** 553
[35] Ebeling W, Förster A, Fortov V, Gryaznov V and Polishchuk A 1991 *Thermophysical Properties of Hot Dense Plasmas* (Stuttgart-Leipzig: Teubner)
[36] Feynman R P and Hibbs A R 1965 *Quantum Mechanics and Path Integrals* (New York: McGraw-Hill)
[37] Filinov V S 1975 *High Temperature* **13** 1065
Filinov V S 1976 *High Temperature* **14** 225
[38] Zelener B V, Norman G E and Filinov V S 1975 *High Temperature* **13** 650
[39] Kelbg G 1963 *Ann. Phys., Lpz.* **12** 219
Kelbg G 1964 *Ann. Phys., Lpz.* **13** 354
Kelbg G 1964 *Ann. Phys., Lpz.* **14** 394
[40] Ebeling W, Hoffmann H J and Kelbg G 1967 *Contrib. Plasma Phys.* **7** 233 and references therein
[41] Herman M F *et al* 1982 *J. Chem. Phys.* **76** 2949
[42] Filinov A V, Lozovik Yu E and Bonitz M 2000 *Phys. Status Solidi* b **221** 231
[43] Filinov A V, Bonitz M and Lozovik Yu E *Phys. Rev. Lett.* **86** 3851
[44] Slattery W L, Dolen G D and De Witt H E 1980 *Phys. Rev.* A **21** 2087

[45] Kahlbaum T 1996 *Physics of Strongly Coupled Plasmas* ed W D Kraeft and M Schlanges (Singapore: World Scientific)
[46] Beule D *et al* 1999 *Phys. Rev.* B **59** 14 177
Beule D *et al* 1999 *Contrib. Plasma Phys.* **39** 21
[47] Militzer B *et al* 2000 *Preprint* Institute of Physics, Humboldt University, Berlin